. Fourth International Symposium of Marine Propellers
smp 15, Austin, Texas, USA, June 2015

Fully Numerical Lifting Line Method for Optimum Propeller Design

Diniz, G.[1]; Brizzolara, S.[2]

[1,2]Department of Mechanical Engineering
Massachusetts Institute of Technology, Boston, MA

Abstract

This paper aims to give a contribution to the design of heavily loaded marine propellers by numerical methods. In this work a wake-adapted lifting line model is used to obtain the optimum circulation distribution along the propeller's blade. This is done via variational method, presented by Coney [1]. In this context, two approaches to the representation of the wake field are compared: the first method utilizes Betz's condition for moderately loaded propellers, in which the wake is aligned with the hydrodynamic pitch angle; and, the second method, in which the wake will be aligned with the local velocities, utilizes Kutta's Law to create a non-lifting wake surface. A brief comparison of the influence of the effect of tip vortex roll-up is done and the results of both methods is submitted to the same lifting surface correction procedures. Finally, the geometries generated in each case is analyzed in a panel method software and the performance of both geometries are compared.

1 Introduction

In the context of potential flow, the lifting line model represents the blades' surface by a line of distributed bound vortices which, integrated along the radius, provides the total thrust required by the hull and the pitch angle of each section. In general, the velocity that each section is subject to is described in the diagram in figure 1 below.

Furthermore, in order to satisfy Kelvin's theorem, the lifting line model must include free vortices shed from the boundaries of bound vortices and extending to infinity downstream of the propeller with equivalent circulation given in equation 1.

$$\Gamma_f(r) = \frac{d\Gamma(r)}{dr} dr \tag{1}$$

A discreet model is idealized by horseshoe elements which extend sufficiently far downstream of the propulsor

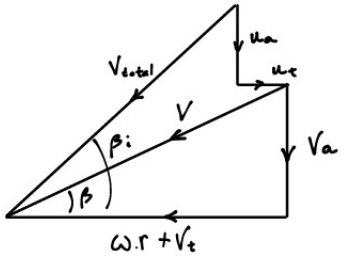

Figure 1: Induced velocities on the lifting line

and with circulations, Γ_f^i, given by equation 2. In this manner, for every bound vortex, there is an upper and a lower free vortex line shed from its boundaries.

$$\Gamma_f^i = \Gamma^{i+1} - \Gamma^i \tag{2}$$

The geometry of these free vortex lines shed downstream are not known a priori and, in general, should be calculated as part of the solution of the design problem. Some approximations valid for moderately loaded propellers have been developed using Betz's condition, equation 3, which prescribes the alignment of the wake field with the hydrodynamic pitch angle calculated at the lifting line.

$$\frac{\tan\beta}{\tan\beta_i} = \eta \cdot \sqrt{\frac{1 - w(xr)}{1 - w_o}} \tag{3}$$

Another approach makes use of Kutta's Law, equation 4, applied to the free vortex lines. These lines should not generate any lift and consequently must be aligned with local velocities.

$$\vec{L} = \rho\vec{\Gamma} \times \vec{V} = 0 \tag{4}$$

Betz's condition has been extensively utilized and studied to model the wake field and has proven to be suitable to design propellers operating in moderately-loaded conditions, as proposed by Lerbs [2]. In addition, Wrench [6] presented asymptotic formulae that provide fast calculations of induced velocities for propeller wakes satisfying Betz's condition, providing reasonably good convergence.

Further, the helicoidal shape of the free vortex lines are simply generated by keeping a constant pitch (hydrodynamic pitch angle) along the free vortex lines shed downstream of the blade, as in figure 2.

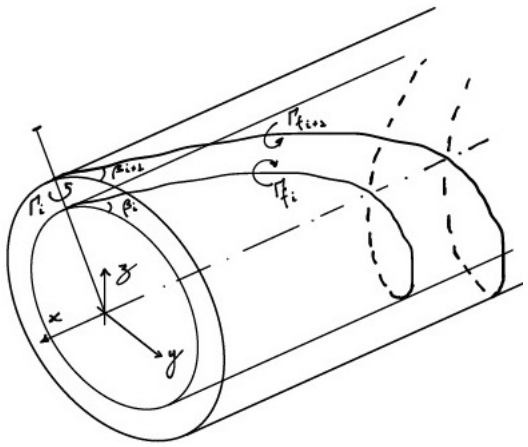

Figure 2: Lifting line model. Bound and trailing vortices

Majority of the lifting line propeller design codes are based on this assumption which turn to be very erratic at higher loading conditions as the constant pitch assumption can not carry any information regarding the effects of tip vortex roll-up or wake radial contraction into the subsequent optimization algorithm.

The significance of these effects has been recently highlighted in the works of Brizzolara et al. [3], with regards to hub effects and Arán and Kinnas [4], with regards to highly loaded conditions. The cited works demonstrate that the shape of the optimum circulation obtained with local velocity alignment may significantly differ from that obtained using the conventional Lerbs (1952)-Wrench (1965) method.

Hence, two approaches to model the lifting line are considered in this work: one in which the wake is aligned with the hydrodynamic pitch angle, to be referred to as Hydrodynamic Pitch Angle Alignment Scheme, or *HPA*; and, the other, in which the wake is aligned with the local velocities, to be referred to as Local Velocity Alignment Scheme, or *LVA*.

This paper investigates the difference between the performance obtained between propulsor geometries obtained using HPA and LVA in order to shed light on the importance of considering tip vortex and wake contraction effects in early stages of design to improve accuracy of results, especially at higher loading conditions. The reference design case in this paper is based on a well known case worked out by Kerwin [5] and reproduced here in table 1.

Table 1: Case test used

r/R	c/D	C_d	Va/Vs	Vt/Vs
0.2	0.17400	0.008	0.880	0.00000
0.25	0.19700	0.008	0.880	0.00000
0.3	0.22900	0.008	0.880	0.00000
0.4	0.27500	0.008	0.880	0.00000
0.5	0.31200	0.008	0.880	0.00000
0.6	0.33700	0.008	0.880	0.00000
0.7	0.34700	0.008	0.880	0.00000
0.8	0.33400	0.008	0.880	0.00000
0.9	0.28000	0.008	0.880	0.00000
0.95	0.24000	0.008	0.880	0.00000
1	0.00200	0.008	0.880	0.00000

Furthermore, in all cases presented here the hub of the propeller was modeled by image vortices method. These image vortices are positioned at a radii, r_v given by equation 5, in which r_t, are the radii of the free vortices.

$$r_v = \frac{r_h^2}{r_t} \tag{5}$$

2 Design Methodology

The design methodology represented in the diagram of figure 3 was utilized in this work. It consists of an iterative method in which the geometrical representation of the lifting line and, most importantly, of the wake field, are used to calculate the induced velocities on the lifting line by the direct application of Biot Savart's Law.

These velocities are used as input for the circulation optimization algorithm also defining the hydrodynamic pitch distribution. The routines then verify the variation of these distributions against the immediate previous step. The relative difference between the circulation or the tangent of the hydrodynamic pitch angle at any point in the radius of the blade is compared to the given tolerance to ensure numerical convergence.

This methodology is applied for both HPA and LVA cases. For the HPA approach, the propeller's wake is aligned with the hydrodynamic pitch angle and is kept fixed along the free vortex lines of the wake. Induced velocities are calculated using the asymptotic formulae proposed by Wrench [6].

For the LVA approach, however, the wake is aligned with the local velocities calculated for each segment in the wake from the direct application of Biot Savart's Law.

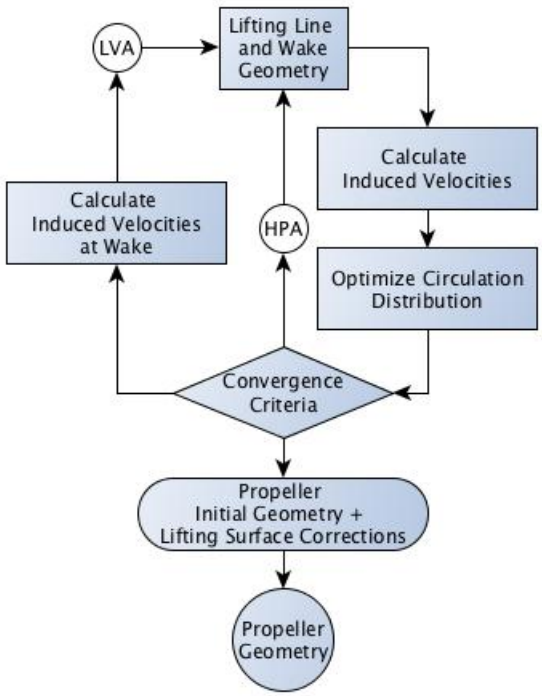

Figure 3: Design Methodology: both HPA and LVA approaches

3 Wake Geometry

3.1 Hydrodynamic Pitch Angle Alignment Scheme (HPA)

Using the HPA approach, the initial geometry of the wake is obtained using the uncorrected angle β, given in equation 6 as the pitch of each free vortex line.

$$\tan\beta = \frac{V_a}{\omega r + V_t} \tag{6}$$

Once the axial, u_a, and tangential, u_t, induced velocities are calculated, the corrected hydrodynamic pitch angle, β_i, is calculated by means of equation 7. The helicoidal lines of the wake's free vortex lines are hence adjusted to this new angle.

$$\tan\beta_i = \frac{V_a + u_a}{\omega r + u_t + V_t} \tag{7}$$

The generated wake geometry with the hydrodynamic pitch alignment scheme is shown in figure 4 for a propeller with $C_T = 1$, $J = 0.8$ and $w_0 = 0.12$.

3.2 Local Velocity Alignment Scheme (LVA)

The algorithm to align the wake with the local velocities consists of calculating the total velocity at the wake field one row of elements at a time and subsequently adjusting the shape of the remaining rows downstream to match the shape of the parent row before.

Initially, the free vortex lines are aligned with hydrodynamic pitch angle. Subsequently, starting from the first row, the total velocity at the control points of the wake are calculated, as per equation 8, where $u_{x,y,z}$ are the cartesian components of the induced velocities and θ is the angle between the Z and Y coordinates of the control points.

$$\vec{V} = (V_a + u_x)\vec{i} + (V_t - \omega.r.\sin\theta + u_y)\vec{j} + (\omega.r.\cos\theta + u_z)\vec{k} \tag{8}$$

The coordinates of the points in the next row are defined by equation 9, where δ_S is the length of the segment linking points X^i and X^{i+1}, as shown in figure 5(a).

$$\vec{X}^{i+1} = \vec{X}^i + \delta_S \frac{\vec{V}^i}{||\vec{V}^i||} \tag{9}$$

The remaining points downstream of that are adjusted so that their shape matches the one at the first row. Once all points downstream are corrected, the procedure then moves to calculate the induced velocities in the second row of elements, and so forth, as shown in figure 5(b). The generated wake geometry with this scheme is shown in figure 6, for a propeller with $C_T = 1$, $J = 0.80$ and $w_0 = 0.12$.

The cross sections of the wake can be visualized in figure 7 (worth noting the sections represented are not equally spaced). The development of the tip vortex roll-up starts at about a quarter turn downstream of the lifting line and is fully developed (third curve from right to left) in one complete turn of the wake.

4 Induced Velocities

4.1 Hydrodynamic Pitch Angle Alignment Scheme (HPA)

The calculation of the induced velocities for the hydrodynamic pitch alignment scheme was made through the use of Wrench's [6] formulae, in which the normalized induction velocities (axial, $\bar{u_a}$, and tangential,$\bar{u_t}$) are calculated by equations 10 and 11.

$$\bar{u_a}(m,i) = \frac{z}{4\pi r_c}\left(y - 2zyy_0F_1\right) \tag{10}$$

$$\bar{u_t}(m,i) = \frac{z^2}{2\pi r_c}\left(y_0F_1\right) \tag{11}$$

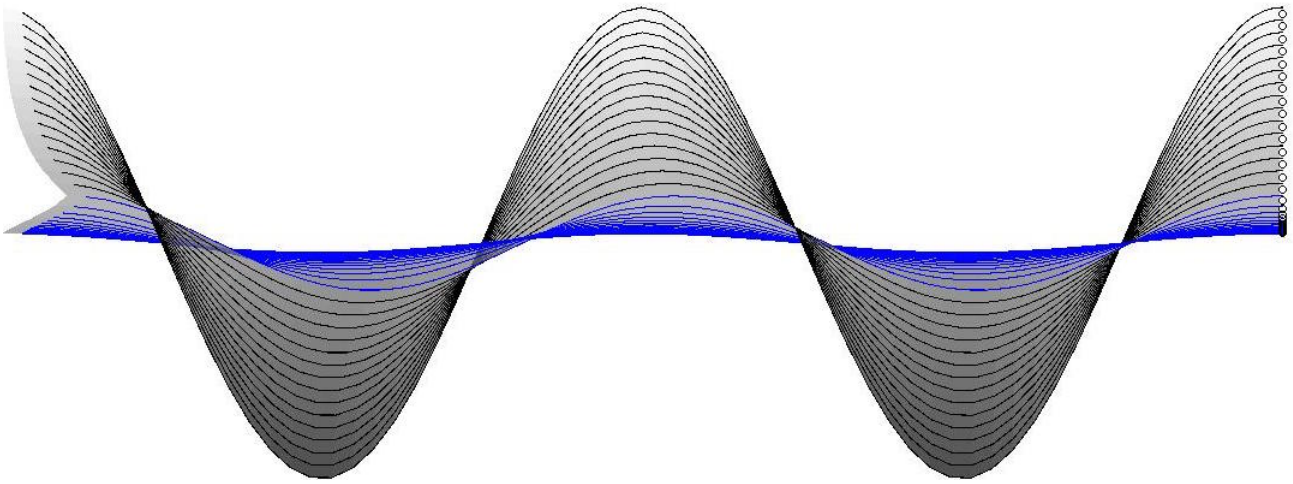

Figure 4: HPA model - $C_T = 1$, $J = 0.80$ and $w_0 = 0.12$

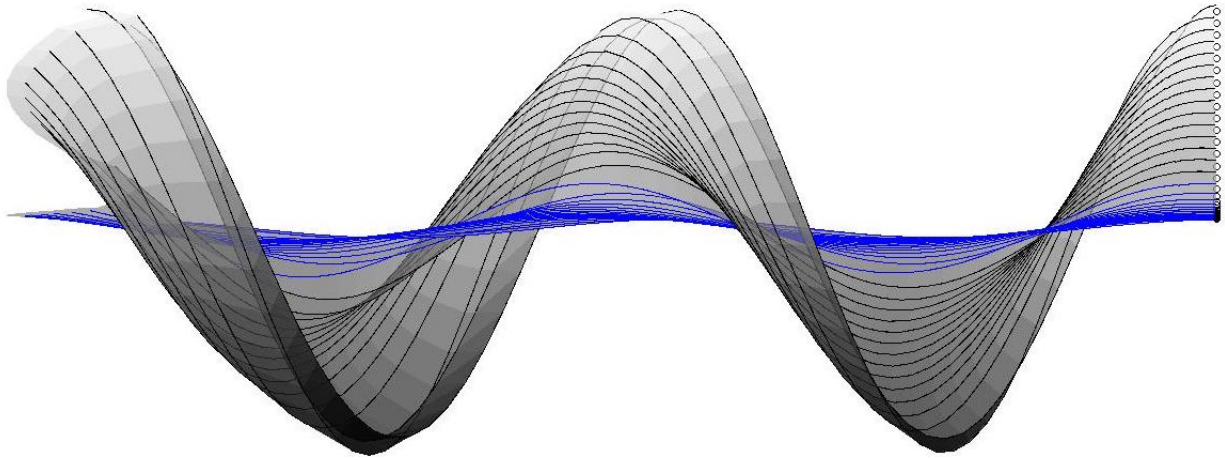

Figure 6: LVA model - $C_T = 1$, $J = 0.80$ and $w_0 = 0.12$

Otherwise, the normalized induced velocities are given by equations 12 and 13.

$$\bar{u_a}(m,i) = -\frac{z^2}{2\pi r_c}\left(y y_0 F_2\right) \tag{12}$$

$$\bar{u_t}(m,i) = \frac{z}{4\pi r_c}\left(1 + 2z y_0 F_2\right) \tag{13}$$

Where,

$$F_1 = -\frac{1}{2Z y_0}\alpha_1\left[\frac{U}{1-U} + \alpha_2.\left(1 + \frac{U}{1-U}\right)\right] \tag{14}$$

$$F_2 = \frac{1}{2Z y_0}\alpha_1\left[\frac{1}{U-1} - \alpha_2.\left(1 + \frac{1}{U-1}\right)\right] \tag{15}$$

And

$$\alpha_1 = \left(\frac{1+y_0^2}{1+y^2}\right)^{\frac{1}{4}} \tag{16}$$

$$\alpha_2 = \frac{1}{24z}\left(\frac{9y_0^2+2}{(1+y_0^2)^{1.5}} + \frac{3y^2-2}{(1+y^2)^{1.5}}\right) \tag{17}$$

$$U = \left(\frac{y_0(\sqrt{1+y^2}-1)}{y(\sqrt{1+y_0^2}-1)}\exp\left(\sqrt{1+y^2} - \sqrt{1+y_0^2}\right)\right)^z \tag{18}$$

$$y = \frac{r_c}{r_v \tan\beta_i} \tag{19}$$

$$y_0 = \frac{1}{\tan\beta_i} \tag{20}$$

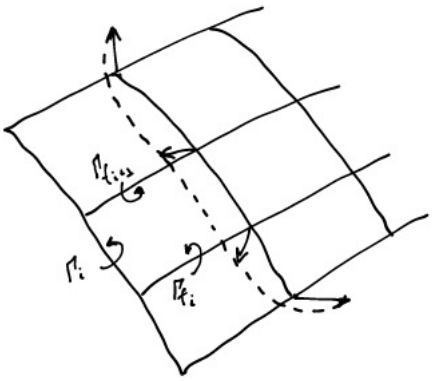

(a) Step 1

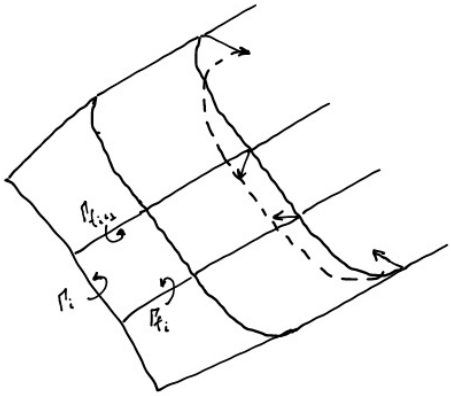

(b) Step 2

Figure 5: Local velocity alignment scheme

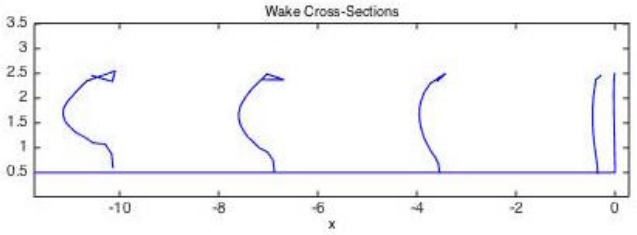

Figure 7: LVA model wake cross-sections

4.2 Local Velocity Alignment Scheme (LVA)

The calculation of the normalized induced velocities for the local velocity alignment scheme was made by means of direct application of Biot-Savart's Law with a Rosenhead-Moore kernel, given by equation 24. This was done in order to smooth the calculations of velocities induced by elements close to each other, which caused instabilities in the calculations.

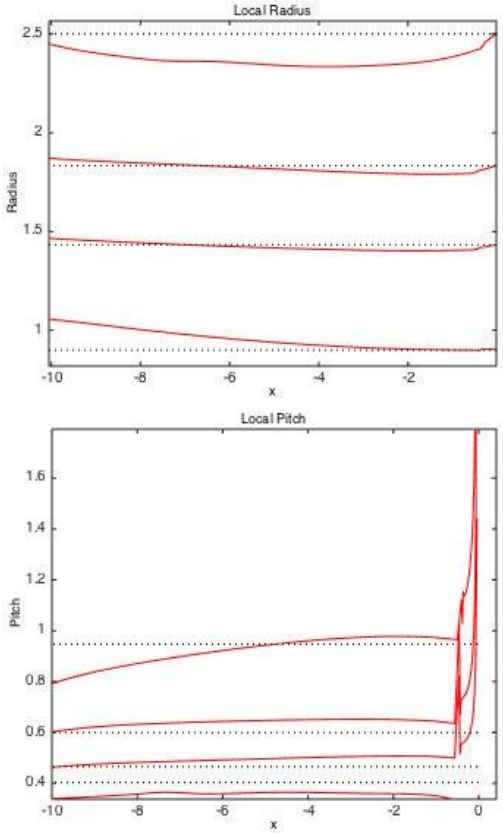

Figure 8: LVA model local pitch and radius variations

$$\vec{u} = \frac{1}{4\Pi} \int \frac{\vec{dl} \times \vec{S}}{\left(||\vec{S}||^2 + \delta^2 \right)^{\frac{3}{2}}} \tag{21}$$

These normalized induced velocities are used as input parameters to the optimization algorithm, described in the following section, to obtain the circulation distribution along the radius of the blade. Once this is done, the induced velocities are calculated by means of equations 22 and 23.

$$u_a(i) = \sum_{m=1}^{M} \Gamma_m \bar{u_a}(m,i) \tag{22}$$

$$u_t(i) = \sum_{m=1}^{M} \Gamma_m \bar{u_t}(m,i) \tag{23}$$

In the LVA approach, however, the calculation of the velocities used for the wake alignment are done by means of equation 24, as in the wake alignment stage of the procedure the circulations are already defined.

$$\vec{u} = \frac{\Gamma}{4\Pi} \int \frac{\vec{dl} \times \vec{S}}{\left(||\vec{S}||^2 + \delta^2 \right)^{\frac{3}{2}}} \tag{24}$$

5 Circulation Optimization

The circulation optimization was performed using the variational method proposed by Coney [1] in which the propeller's thrust and torque are obtained by numerical integration of the lift and drag forces generated at each section. As a result, the total thrust and torque are calculated by means of equations 25 and 26.

$$T = \rho Z \sum_{m=1}^{M} \left[(V_t(m) + \omega r_c(m) + u_t(m)) \right] \Gamma(m) \Delta r - \rho Z \sum_{m=1}^{M} \left[\frac{1}{2} V \left(V_a(m) + u_a(m) \right) c(m) C_{dv}(m) \Delta r \right] \tag{25}$$

$$Q = \rho Z \sum_{m=1}^{M} \left[(V_t(m) + \omega r_c(m) + u_t(m)) \right] \Gamma(m) r(m) \Delta r - \rho Z \sum_{m=1}^{M} \left[\frac{1}{2} V \left(V_a(m) + u_a(m) \right) c(m) C_{dv}(m) r(m) \Delta r \right] \tag{26}$$

With the expressions for thrust and torque, it is possible to define an auxiliary function, H, in accordance with the calculus of variations, in which T_r is the required thrust of the propeller.

$$H = Q + \lambda (T - T_r) \tag{27}$$

Taking the expressions of the partial derivatives of H, with respect to all Γ_i and to the Lagrange multiplier, one can obtain the system that provides the optimum circulation distribution to maximize efficiency (minimizing torque) while respecting the constraint of the required thrust, T_r.

$$\frac{\partial H}{\partial \Gamma_i} = 0 \tag{28}$$

$$\frac{\partial H}{\partial \lambda} = 0 \tag{29}$$

This is a non-linear system as the multiplication of the terms $\Gamma.u_t$ in 25 and the terms $V.V_a$ in the viscous part of 26. Linearization is obtained by rewriting these expressions, making the terms u_t^* and V^* fixed and assuming an initial value for the Lagrange multiplier λ.

After every solution of the linearized system of equations, the values of Γ_i and λ are used to obtain the new values of u_t^*, V^* by equations 22 - 23 and 8, respectively.

6 Convergence Analysis

The methodology described in figure 3 is applied for both HPA and LVA cases using a propeller with $C_T = 1$, $J = 0.80$ and $w_0 = 0.12$. As seen in figures 9 and 10, respectively, the convergence of the methods in terms of velocities and circulation is very fast. The relative error represented in these graphs are calculated as the maximum relative difference between the current iteration and the first one.

In this work a tolerance of 0.1% was utilized, but this value was rather arbitrary and it could be smaller without prejudice of accuracy. The number of iterations necessary to achieve the required tolerance, however, is non linear with respect to the tolerance chosen.

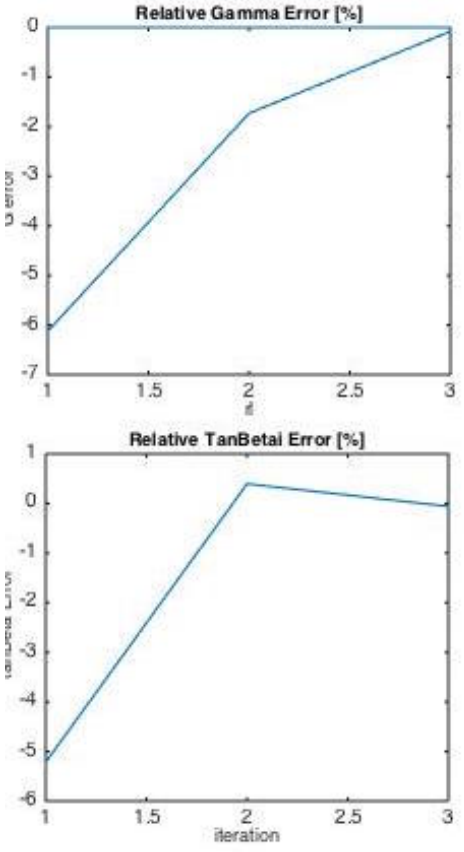

Figure 9: HPA convergence of the error on circulation and the induced velocities

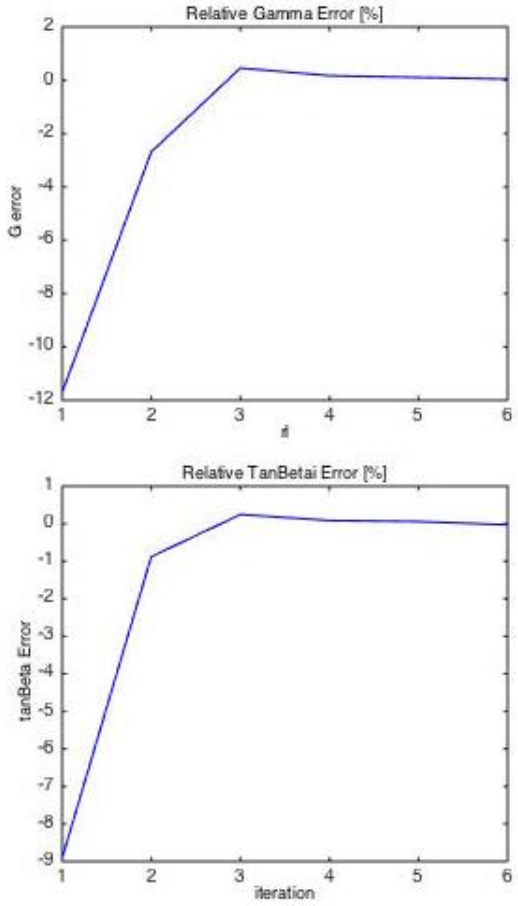

Figure 10: LVA convergence of the error on circulation and the induced velocities

7 Comparison of Results

An initial comparison between the results of the two methods shows that the approaches present significant differences both in the distributions of circulation and hydrodynamic pitch angle.

As a general rule, the LVA approach seems to attribute higher loads at the root and decrease the loading at the tip. The hydrodynamic pitch angle shows equally or even more significant differences between the methods.

The HPA method presents significantly lower pitch angles both at the root and at the tip sections of the blades in comparison with the results using the LVA approach, as these areas are more directly affected by vortex shedding effects.

8 Propeller Initial Geometry

Once convergence is achieved, the initial geometry of the propeller, that is, the initial distribution of camber, angle of attack and geometric pitch angle is obtained. The circulations, Γ_i, and chords, c, are used to define the lifting coefficient of each section.

$$c_{Li} = \frac{2\Gamma_i}{V_i c_i} \tag{30}$$

The total lift is generated at each section by both camber and angle of attack. In order to ensure a sufficient margin to face cavitation, it is usually assumed that a proportion of p = 90% of the total lift is generated by camber and the remaining lift by angle of attack.

Hence, the angle of attack can be defined by equation 31, in which the slope of the $c_L - \alpha$ curve of the foil is assumed constant and equal to 2π.

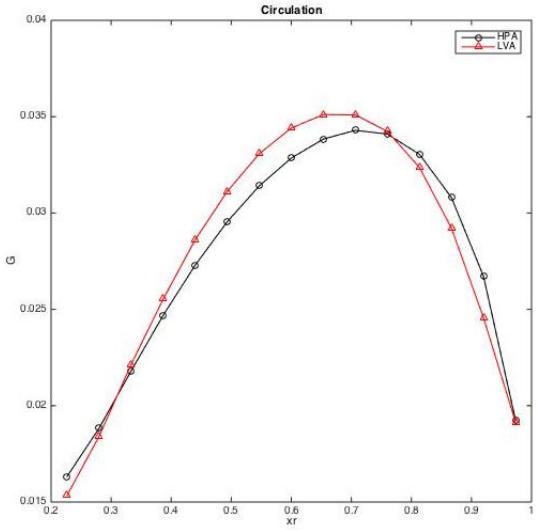

(a)

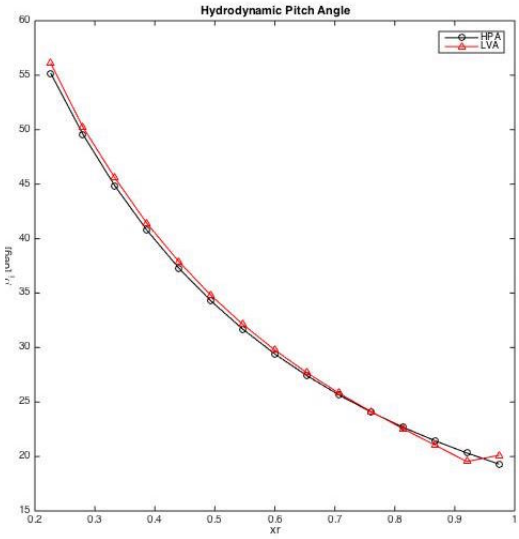

(b)

Figure 11: Comparison of results

$$\alpha_i = \frac{c_{Li}.(1-p)}{2.\pi} \tag{31}$$

The maximum camber of the section is defined by equation 32, in which K_t and K_f are the coefficients defined by Castagneto and Maioli [9], and m_{Ti} are the maximum thicknesses of each section, (taken from table 1).

$$f_i = \frac{c_i p. c_{Li}}{(K_f(1 + K_t(\frac{m_{Ti}}{c_i}))} \tag{32}$$

Using a NACA16 thickness line with a mean line a = 0.8, the geometry of each foil that defines the sections of the propeller are obtained.

Last, the chord and thickness distributions were obtained using the method described by Brizzolara et al. [8] in which criterion for strength and cavitation are simultaneously imposed on the propeller in a iterative manner to optimize these distributions along the span of the blade.

The results obtained for the propeller in the HPA case with $C_T = 1$, $J = 0.80$ and $w_0 = 0.12$ are presented in figure 12.

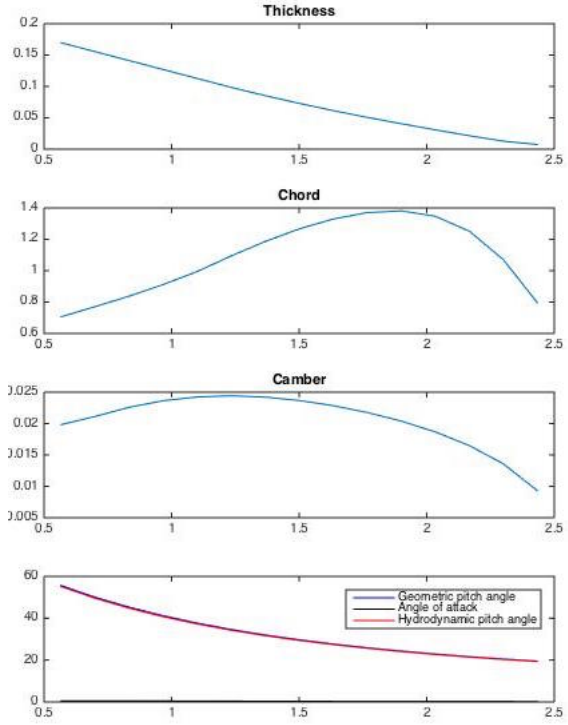

Figure 12: Initial Geometry

9 Lifting Surface Corrections

With this initial geometry, corrections on angle of attack and maximum section camber can be made by modeling the geometry of the propeller by a zero thickness lifting surface.

In this model, horseshoe elements are positioned along the chord of the blade and free vortex lines are shed downstream similarly to the lifting line model. The integrated circulation along the chord of each section must be equal to the total circulation given by the lifting line in that section, as in equation 33

$$G(r,\theta) = \int_{\theta_l}^{\theta_t} G_r(r,\theta) d\theta \tag{33}$$

And, again, to satisfy Kelvin's theorem, the strength of the circulation of the free vortex lines is given by equation 34.

$$G_f(r,\theta) = -\frac{dG(r,\theta)}{dr} dr \tag{34}$$

Substituting equation 33 into 34 one gets:

$$\begin{aligned} G_f(r,\theta) = -\frac{d}{dr}\int_{\theta_l}^{\theta_t} \frac{\partial G_r}{\partial r} d\theta dr - \\ G_r(r,\theta_l)\frac{d\theta_l}{dr} dr - \\ G_r(r,\theta_t)\frac{d\theta_t}{dr} dr \end{aligned} \tag{35}$$

From which the induced velocities are then calculated by means of direct application of Biot Savart's Law in equation 36.

$$\begin{aligned} \frac{V_t}{V_r}(P) = -\frac{1}{2}\left[\iint_{A1} G_r(r,\theta)\frac{\vec{S}\times\vec{r}}{||\vec{S}||^3} d\theta dr + \right. \\ \left. \iint_{A_1+A_2} G_f(r,\theta)\frac{\vec{S}\times\vec{r}}{||\vec{S}||^3} d\theta dr\right] \end{aligned} \tag{36}$$

And with some algebraic manipulations, one can obtain the expression for the normalized induced velocities from the lifting surface in equation 37.

$$\begin{aligned} \left[\frac{U_n}{V_r} - \frac{U}{V_r}\right] = -n\cdot\left[\sum_1^z \iint_{A1} G_r(r,\theta)\frac{\vec{S}\times\vec{r}}{||\vec{S}||^3} d\theta dr\right] + \\ n\cdot\left[\sum_1^z \left[\iint \left(G_r(r,\theta_t)\frac{d\theta_t}{dr} + \int_\theta^{\theta_l}\frac{\partial G_r}{\partial r} d\theta dr\right)\frac{\vec{S}\times\vec{r}}{||\vec{S}||^3} dr\right]\right] \\ - n\left[\cdot\iint \frac{dG}{dr}(r,\theta)\frac{\vec{S}\times\vec{r}}{||\vec{S}||^3} dr\right] \end{aligned} \tag{37}$$

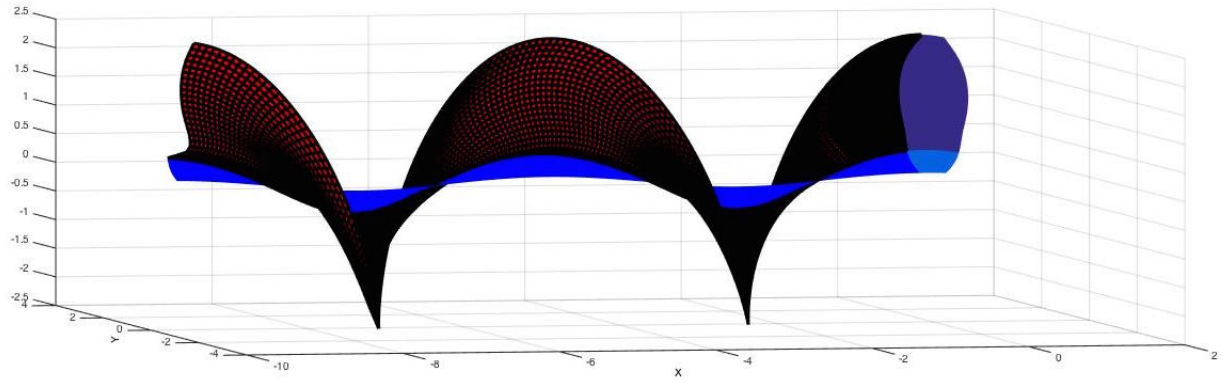

Figure 13: Lifting surface model

where:

$$\frac{U}{V_r} \rightarrow \text{induced velocities from lifting line}$$

The new mean line of each section is reconstructed by its alignment with the total inflow velocity (now, including the velocities calculated by the lifting surface) and the geometry of the lifting surface model shown in figure 13 is used to obtain the maximum camber and angle of attack distributions.

In figures 14 and 15, the resulting corrections and final vales of both camber and angle of attack, respectively, are presented for the propeller obtained with LVA approach, with $C_T = 1$, $J = 0.80$ and $w_0 = 0.12$.

10 Performance Analysis and Comparison

10.1 Lifting Surface Corrections

To verify the results obtained by the two different design approaches, an analysis of the two different propeller geometries was performed by a higher fidelity numerical method. To the purpose, a low order boundary element method with flow aligned wake capability [10], extensively validated over different types of propellers (e.g. [11] [12]), was used.

The analysis was aimed to assess the fulfillment of the design requirements by the fully numerical lifting line model and, at the same time, to assess if the higher fidelity method which allows for the exact geometric features of the propeller (in particular camber, thickness distribution along the chord and hub wasll effect) could predict the same performance variations between the HPA and LVA cases.

The propeller geometries are those already presented obtained from the design methods from the initial input data of table 1, considering 5-bladed propeller, $z = 5$, a diameter $D = 5m$.

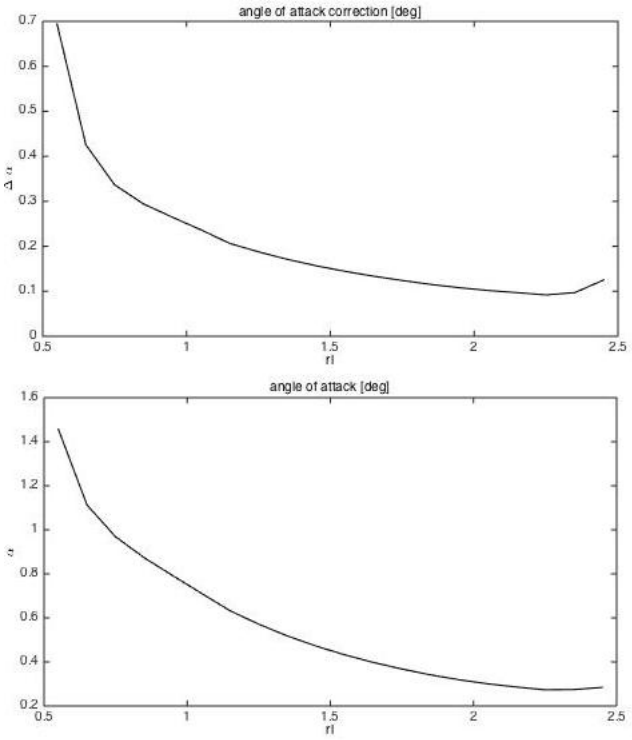

Figure 14: Lifting surface angle of attack correction and final distribution

The results of this analysis are summarized in table 2, presenting the thrust and torque coefficients and the efficiency of the propellers obtained for both the HPA and LVA cases, and for each case, including or not lifting surface corrections in the methodology to derive the propellers geometry characteristics.

The data points to a decrease in efficiency while including the effects of wake alignment in the optimization procedure. The HPA presented about 1.2% in reduction of efficiency compared to HPA cases.

This decrease in efficiency is likely to be directly related to the effects of the tip vortex roll-up once both

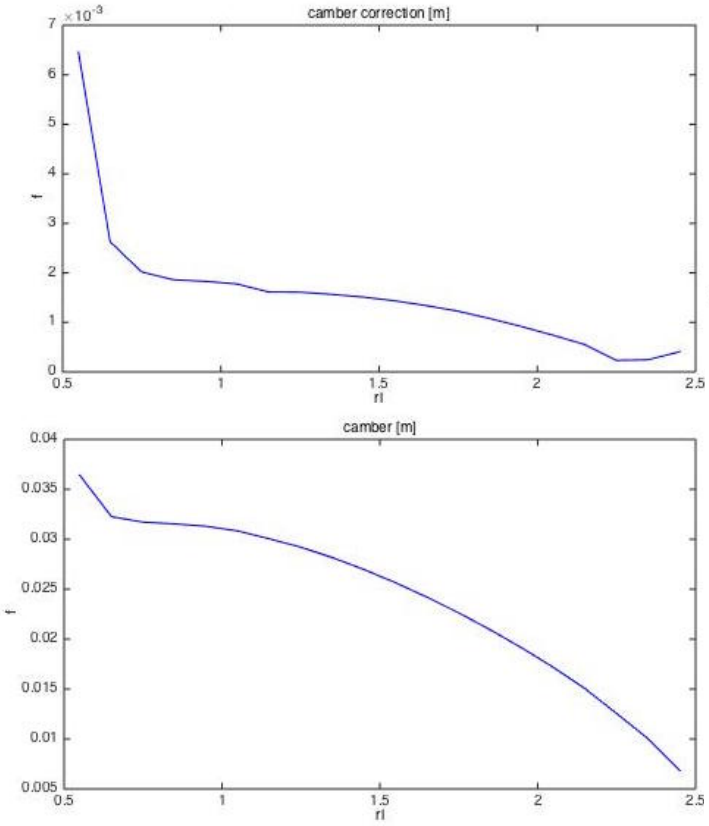

Figure 15: Lifting surface camber correction and final distribution

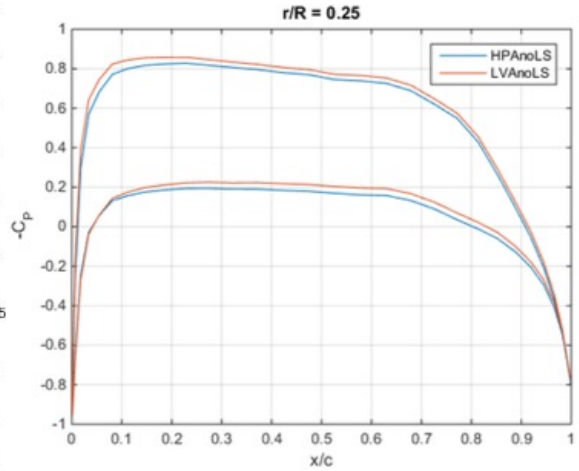

(a)

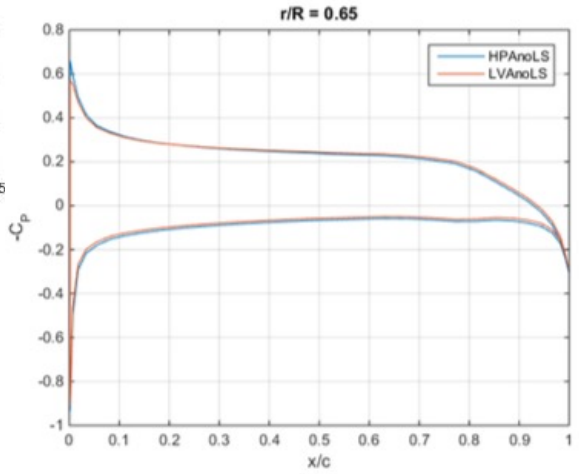

(b)

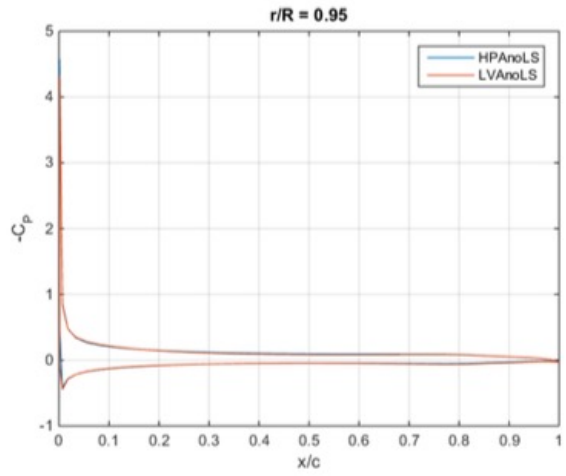

(c)

Figure 16: Pressure coefficient distribution at different radii of the blade

geometries were subject to the same design criteria, with exception of the geometry of the wake. Furthermore, the sections of the blades seem to be working equivalently well in terms of alignment of the local velocities, as seen in figure 16. This is due to the pitch and camber corrections of the lifting surface model

The pressure coefficient distribution along the chords of the blade sections, whose geometry was obtained excluding lifting surface corrections, shows a common trend experienced by both geometries.

This indicates their operation to be comparable, at least from what can be inferred with a potential flow based analysis, which leads to the obvious conclusion that the effects of the wake alignment with the local velocities plays an important role in the operation of heavily-loaded propellers.

The panel method also showed significant differences in terms of circulation and induced velocities between the HPA and LVA designes. The variation in thrust coefficient between LVA and HPS predicted by the panel emthod is nearly 3% .

As expected the closest thrust to the design value is achieved by the propeller LVA with lifting surface corrections, as predicted by the panel method. This confirms

the closer fidelity of the fully numeric lifting line model with flow adapted vortical wake.

In addition, the comparison between the effects of lifting surface correction in the final performance of the propeller was analyzed and, as the data shows, the total thrust produced by propellers submitted to lifting surface correction procedure in comparison with those which have not is generally higher in comparison to those which were not.

The increase in thrust is mainly due to the increase of camber and to a lesser extent to the angle of attack distributions added by the lifting surface method. This is observed in figures 18 and 19 and it is in accordance with the initial design philosophy adopted to have a larger margin on the possibility of face cavitation by assigning a 10% lift contribution to angle of attack.

The lifting surface corrections, obtained with the presented method which considers the hub effects, tend to increase the angle of attack of the root sections and decrease their maximum camber. The result of this correction appers right as confirmed by the correct shapes of pressure distribution for the profiles at the blade root, as for instance presented in 16, for $r/R = 0.25$ (a).

The increase in thrust is also observed in the comparison of the circulation distributions , as seen in figures 17 and 20, between HPA and LVA cases.

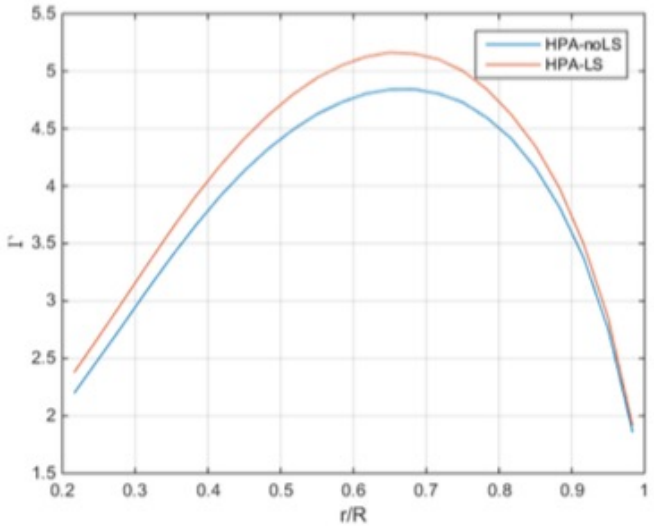

Figure 17: Comparison of circulation distributions due to lifting surface corrections for HPA approach

For the HPA case in which lifting surface corrections were performed, however, the relative error is slightly increased to 5.7% in comparison with the case in which no corrections were made.

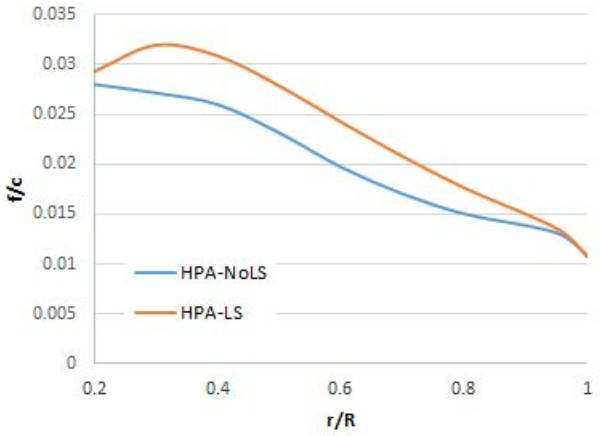

Figure 18: Comparison of camber distributions due to lifting surface corrections

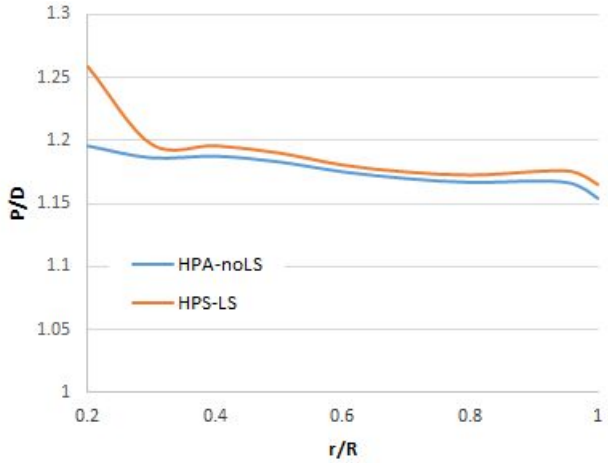

Figure 19: Comparison of geometric pitch distributions due to lifting surface corrections

Table 2: Comparison of results

Method	KT	10.KQ	η
Lifting line			
HPA	0.2532	0.4064	0.8000
LVA	0.2532	0.4105	0.7950
Panel method			
HPA˙noLS	0.2529	0.4497	0.7161
HPA˙LS	0.2657	0.4780	0.7079
LVA˙noLS	0.2472	0.4453	0.7068
LVA˙LS	0.2589	0.4721	0.6981

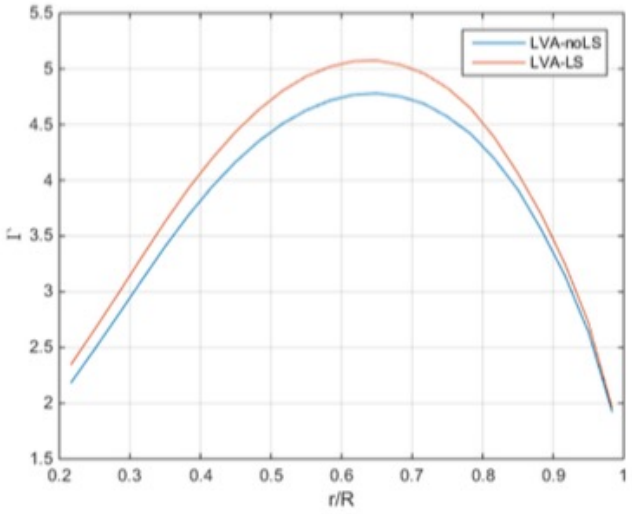

Figure 20: Comparison of camber distributions due to lifting surface corrections for LVA approach

11 Conclusions

In this work, the systematic methodology utilized to design wake adapted propellers under heavily-loaded operation has shown the importance in considering the effects of tip vortex roll-up in early stages of design. The comparison of the efficiencies obtained by the HPA method with those obtained by the LVA method indicates a significant decrease in efficiency when the effects of the aligned wake are considered through the fully numerical method (LVA). This observed trend goes in the right direction, i.e. it tends to bring the efficiency estimated by the lifting line down to more realistic values.

Furthermore, the comparison between of results obtained between cases in which lifting surface corrections were not performed, with those in which they were, clearly points out to the importance of including those effects in design stages of propeller design.

The data observed in this paper show that by neglecting the effects of wake tip vortex roll-up (that is by designing the geometry of the wake using Betz's condition) the designer might incur in a significant overestimation of the propeller thrust and in a non-correct load distribution along the radius. In addition, only when the proposed fully numerical lifting line method is combined with lifting surface corrections that consistently consider the wall effect induced by the hub presence, the methodology seems able to provide a propeller geometry that achieves the initial design thrust requirements.

In the coinsidered design case of a heavily loaded propeller, $C_T = 1$, the global correction of thrust given by the lifting surface method induce an increase of thrust of about 4%, while the use of the fully numerical lifting surface method reduces it by about 3%, getting the closest result to the design value, also in terms of radial load distribution (especially close to the tip and the hub).

12 Acknowledgements

The present work has been partially supported by scholarship at the Massachusetts Institute of Technology sponsored by the American Bureau of Shipping.

References

[1] Coney, W. B. *A Method for the Design of a Class of Optimum Marine Propulsors.* PhD thesis, Massachusetts Institute of Technology. 1989.

[2] Newman, J.N. *Moderately loaded propellers with a finite number of blades and an arbitrary distribution of circulation.* SNAME Transactions, 60, 73-123. 1952.

[3] Brizzolara S., Gaggero S., Grassi D. *Hub Effect in Propeller Design and Analysis* Third International Symposium on Marine Propulsors, smp′13, Launceston, Tasmania, Australia, 2013. Vol.1, pp.110-119. ISBN: 978-0-646-90334-7.

[4] Arán D.H.M., Kinnas S.A. *On Fully Aligned Lifting Line Model for Propellers: An Assessment of Betz condition.* Journal of Ship Research, Vol. 58, No. 3, September 2014, pp. 130-145. 2014

[5] Kerwin, J. E., Hadler, J.B. *The Principles of Naval Architecture Series - Propulsion. p. 92* SNAME Publications. 2010

[6] Wrench, J. W. *The calculation of propeller induction factors.* TR-1116, DTMB, Bethesda, MD. 1957

[7] Morgan, W.; Wrench, J. *Some Computational Aspects of Propeller Design. Methods in Computational Physics.* New York: Academic Press, pp. 301-31. 1965.

[8] Brizzolara S., Grassi D., Tincani E.P. *Design Method for Contra-Rotating Propellers for High-Speed Crafts: Revising the Original Lerbs Theory in a Modern Perspective.* International Journal of Rotating Machinery, Volume 2012, Article ID 408135, 18 pages. doi:10.1155/2012/408135.

[9] Castagneto E., Maioli P.G. *Theoretical and Experimental Study on the Dynamics of Hydrofoils as Applied to Naval Architecture.* Proceedings of the 7th Symposium of Naval Hydrodynamic, Rome, Italy, 1968.

[10] Gaggero S., Brizzolara S. *Exact Modeling of Trailing Vorticity in Panel Method for Marine Propeller.* Proceedings of 2nd International Conference on Marine Research and Transportation. Ischia, 28-30 June 2007, Univ. Federico II, ed., p. D-1-D-9, ISBN/ISSN: 88-901174-3-5.

[11] Brizzolara S., Villa D., Gaggero S. *A Systematic Comparison between RANSE and Panel Method for Propeller Analysis.* Hydrodynamics VIII, Proceedings of the 8th International Conference on Hydrodynamics, ICHD 2008. Nantes, Oct. 2008, vol. 1, p. 289-302.

[12] Gaggero S., Villa D., Brizzolara S. *SMP Workshop on Cavitation and Propeller Performances: The Experience of the University of Genoa on the Potsdam Propeller Test Case.* Proceedings of the Workshop on Cavitation and Propeller Performance. Second International Symposium on Marine Propulsors - smp′11. Hamburg, 17 June 2011, vol. 1, p. 92-105, ISBN/ISSN: 978-3-86342-238-7.

Index